5-1-2024

Manufacturing, characterization, and macromechanical modeling of short flax/hemp fiber-hybrid reinforced polypropylene

Bilel Miled
Pôle Universitaire de Montfoulon

Slim Kammoun
Université de Tunis El Manar, Ecole Nationale d'Ingénieurs de Tunis

Imane Belyamani
Zayed University, imane.belyamani@zu.ac.ae

Laurent Cauret
Pôle Universitaire de Montfoulon

Forces in Mechanics 15 (2024) 100269

Contents lists available at ScienceDirect

Forces in Mechanics

journal homepage: www.sciencedirect.com/journal/forces-in-mechanics

Manufacturing, characterization, and macromechanical modeling of short flax/hemp fiber-hybrid reinforced polypropylene

Bilel Miled [a,*], Slim Kammoun [b,c], Imane Belyamani [d,*], Laurent Cauret [a,e]

[a] Polyvia Formation, Polyvia Polymers and Composites Research (2PCR), Pôle Universitaire de Montfoulon, BP 823, 61041 Alençon Cedex, France
[b] Université Tunis El Manar, Ecole Nationale d'Ingénieurs de Tunis, Laboratoire de Génie Civil, BP 37, 1002 Tunis, Tunisia
[c] National Engineering School of Sfax, University of Sfax, Sfax, Tunisia
[d] College of Natural and Health Sciences, Zayed University, P. O. Box 144534 Abu Dhabi, United Arab Emirates
[e] Institut des Molécules et Matériaux du Mans (IMMM), UMR 6283 CNRS – Le Mans Université, Avenue Olivier Messiaen, 72085 Le Mans Cedex 9, France

ARTICLE INFO

Keywords:
Flax
Hemp
Hybrid composites
Damage mechanism
Mechanical characterization
EVP constitutive model
Perzyna-type model

ABSTRACT

The present work focuses on the manufacturing, mechanical characterization, and modeling of hybrid Flax/Hemp/Polypropylene (PP) composites under dry conditions. Geometric parameters of the fibers were measured both before and after the melt processing. The results indicated that the processed fibers, especially the hybrid ones, had a narrowed length distribution with an average fiber length of 0.48 mm for hybrids compared to 0.62 mm for non-hybrids. The hybrid composites were mechanically characterized using basic and loading-unloading tensile tests with various fiber combinations and weight percentages. The study also examined the effect of strain rate and cutting angle on the behaviors of the composites. The results demonstrated the significance of fiber orientation as the primary factor in explaining mechanical variations. The tensile strength and Young's Modulus of FH30 composites (PP + 15 wt% flax + 15 wt% hemp) increased by about 24.1 % and 10.9 %, respectively, when the plates were cut into dumbbell shapes at a 90° angle to the injection molding flow direction, compared to a cut at 0° The study also showed that the tensile strength is directly proportional to the mass fraction of reinforcements, with an increase in tensile strength by 7.9 % for 0° cut angle specimens between FH10 (PP + 5 wt% flax + 5 wt% hemp) and FH30 bio-composites, while the uniform strain is inversely proportional to the mass fraction of reinforcements, evidenced by a reduction in uniform strain of 30 % between FH10 and FH30 samples. Morphological observations revealed the presence of bands indicating the propagation of micro-cracks, as well as debonding or cohesive failure. Finally, a Perzyna-type elasto-viscoplastic constitutive model was applied to accurately predict the overall mechanical response of a hybrid composite material. Specifically, the model successfully captured the tension deformation behavior of hybrid natural short-fiber thermoplastic composites, including the elastic stage, yield stress, and nonlinear hardening.

1. Introduction

Bio-composites are defined by the inclusion of one or more materials (fibers or matrices) obtained from natural sources. Although natural fiber-based thermoplastic composites are known to have inferior mechanical properties compared with thermoset composites, they have advantages for design flexibility, great capacity to be recycled, and are consumed in large volumes.

For this type of composite, polypropylene (PP) is widely used as a polymer matrix due to its versatility, low density, resistance to damage, non-toxicity, and low cost. In addition, the processing ease of PP, with its low melt viscosity, makes it highly suitable for injection molding applications. Like every other polymer, polypropylene has a few disadvantages compared with some thermosets: it has high flammability, poor adhesion properties, and it is susceptible to UV degradation and oxidation.

Natural fibers are classified into three categories based on their origin, namely plant fibers, animal fibers and mineral fibers. Nonwoven bio-composites can be manufactured from a large range of plant fibers, but the most commonly used fibers are flax, hemp, or jute. These natural fibers offer similar strength and stiffness to glass fiber, presenting opportunities to replace synthetic fibers in semi-structural automotive parts and in applications requiring high-vibration damping, such as sporting goods and musical instruments [1,2,3]. Additionally, they

* Corresponding authors.
E-mail addresses: b.miled@polyvia-formation.fr (B. Miled), imane.belyamani@gmail.com (I. Belyamani).

https://doi.org/10.1016/j.finmec.2024.100269
Received 25 September 2023; Received in revised form 8 March 2024; Accepted 10 April 2024
Available online 13 April 2024

possess enormous advantages compared to E-glass fibers such as low density, renewable resources, short growth cycle times, low energy production, recyclability, biodegradability, and excellent specific mechanical properties that are equivalent to those of glass fibers.

Despite the interesting specific properties of natural fibers, they exhibit certain drawbacks compared to conventional fibers (glass fiber). These disadvantages include lower thermal stability (this limits the manufacturing process and the choice of the polymers), higher moisture absorption, and lower mechanical performance. These disadvantages limit the use of natural fibers as reinforcements in composite materials.

Flax (*Linum usitatissimum*) and Hemp (*cannabis*) are the major plant fibers cultivated in northern Europe and are mainly used in the textile sector. Considering the interesting properties of these two natural fibers, hybridization, which consists of two or more types of fibers in the same composite system could be used to provide additional benefits, including greater energy absorption and lower cost [4].

Several studies have been carried out to explore the mechanical properties of natural/synthetic or natural/natural binary hybrid fibers reinforced laminate composites. These include research on flax fiber combined with glass fiber [5,6,7,8,9,10], flax fiber combined with carbon fiber [11,12,13], and flax fiber combined with basalt fiber [14,15,16,17]. Other studies have investigated the hybridization of three fiber types embedded in a common matrix such as abaca/jute/glass fibers [18], flax/banana/glass fibers [19], jute/banana/glass fibers [20], and flax/basalt/glass woven fabrics reinforced epoxy composites laminate fabricated using vacuum bagging process [21,22,23]. However, only a few studies have examined the hybridization of four or more fiber types in the same composite system. Notable among these, is the research work assessing the mechanical performance of laminated composites based on basalt/flax/hemp/glass fibers [24,25]. Additionally, other studies have assessed the mechanical properties (tensile, flexural, in-plane shear, interlaminar shear and bearing properties) of hybrid fiber metal laminates (FMLs) which are constructed by sandwiching a hybrid fiber-reinforced composite between thin layers of metals with aluminum as the metal component and jute, glass, aramid, carbon, and basalt fabrics as composite components [26,27,28]. The aforementioned studies investigated the mechanical, thermal, and damping properties of hybrid laminated composites made from a combination of natural fibers (e.g. flax, jute, and abaca) and synthetic fibers (e.g. glass, carbon, and basalt). The findings suggested that increasing the concentration of glass, carbon, or basalt fibers enhances the tensile and flexural properties and that hybrid composites offer superior mechanical performance compared to mono-composites. The layer arrangement significantly affects the tensile strength and failure strain, while leaving the modulus unchanged. Additionally, flax layer positioning was shown to impact both the bending stiffness and damping. Hybridization has been demonstrated to enhance fracture toughness, interlaminar shear strength, thermal stability, and water repellence. On the other hand, hybrid laminated composites provide exceptional damping capabilities and reduce weight while maintaining specific mechanical properties.

The macroscopic behavior of short natural fiber reinforced composites (SNFRCs) with a PP matrix is strongly related to three factors: nature and physico-chemical characteristics of the matrix, reinforcement, and fiber/matrix interfacial bonding (quality of the fiber/matrix adhesion, contact surface). The mechanical and physico-chemical properties of flax and hemp fibers vary according to the fiber orientation [29,30,31], the aspect ratio of the fiber reinforcement [32], the volume or mass fraction of fibers, and the processing temperature of the thermoplastic composites.

For the assessment of the (visco)elastic and visco(plastic) characteristics of aligned/nonaligned short-fiber composites, many modeling approaches of varying accuracy and complexity were applied [33]. The numerical modeling of these composites is possible at different scales: micro, *meso*, and macro-scale [34]. For instance, Sandberg and Rydholm [35] investigated the impact response during two complex load cases and compared the results of a simple elastoplastic material law and failure model with a more complex crash model, while Chethan et al. [36] used a bilinear material model defining yield strength and tangent modulus for hemp polyester composites. Puech et al. [37] developed an original method for the characterization and prediction of the impact behavior of short hemp fiber-reinforced biocomposites through the combination of experimental impact testing, high-speed imaging, and finite element modeling. A macroscopic non-linear material model was used to describe the material behavior during impact and a strain-based erosion criterion was used to model damage. Kebir and Ayad [38] proposed another approach based on a multi-scale numerical model, named 'Projected Fibers (PF)', to estimate the macroscopic elastic properties (Young's modulus, Poisson's ratio, shear modulus, …) of reinforced hemp fiber polypropylene composites, from those of their components (matrix and fibers). The model uses a specific finite element procedure which is associated with a random distribution of short fibers, and it considers the geometry and the mechanical properties of composite components. Shu and Stanciulescu [39] proposed a finite element framework based on the development of representative volume element (RVE) and an analytical homogenization strategy for the characterization of SNFRCs with flax fiber and PP matrix, followed by a study on the influence of imperfect interfaces and complex microstructures on the effective properties of the composites. Kern et al. [40] used aligned/non-aligned-fibers finite element analysis (FEA) models to explore the stress fields within the matrix and fibers and along the fiber-to-matrix interface. These models are configured to the geometric and elastic properties of wheat straw fiber and PP matrix. Pan and Zhong [41] developed a nonlinear constitutive model of SNFRCs with sisal fibers and PP matrix to describe the kinetic processes of moisture absorption and mechanical degradation. These correlated thermodynamic processes have been described by introducing an internal variable to reflect the energy dissipation. Modniks and Andersons [42] applied an orientation averaging technique to numerically predict the non-linear stress–strain diagrams in the tension of a flax/polypropylene composite with different fiber volume fractions. A unit-cell single-fiber FEA was created, and the result of a single model was used to obtain the mechanical behavior of the multi-fiber model by orientation averaging technique. Sliseris et al. [43] developed a micromechanical model to generate and simulate the mechanical properties of flax short fiber-reinforced polymer composites. The fiber defects and the interfacial zones of fiber bundles are modeled using a nonlocal isotropic continuum brittle damage model whereas the PP matrix is modeled by a non-linear standard Mises plasticity model with an isotropic hardening law.

In this paper, a phenomenological Perzyna elasto-viscoplastic constitutive law is applied to forecast the hybrid composite's macroscopic behavior, and a material parameter adjustment approach is employed to select the hardening law and viscoplastic function that best describes the hybrid composite's behavior. To the best of the authors' knowledge, limited research has been conducted on the performance evaluation of hybrid fiber-reinforced composites incorporating flax and hemp fibers in a PP matrix. The primary focus of these studies revolved around the investigation of laminated composite materials [44,45]. The significance and originality of this research work lie in the integration of multiple aspects. First, it involves the hybridization of short hemp and flax natural fibers as reinforcements within a polypropylene matrix, implemented through the injection molding process. Second, the study stands out for its extensive mechanical characterizations, encompassing fiber orientation, fiber geometry, strain rate effects, and damage mechanisms, particularly in the context of both simple and load/unload tensile tests. These characterizations offer valuable insights into the strength capabilities, stiffness, and failure modes of the hybrid natural fiber composites. Finally, the application of an elasto-viscoplastic (EVP) constitutive law underscores a commitment to accurately capturing the intricate mechanical behavior of these composites. This constitutive model goes beyond the conventional considerations of linear elasticity and plasticity, incorporating time-dependent mechanical

characteristics, resulting in a more comprehensive understanding.

Expanding upon these remarkable technical advancements, these bio-composites show the potential for substituting synthetic fiber composites in a wide range of lightweight and low-cost applications [46,47]. They represent a sustainable solution for various applications, including materials for insulation and furniture, household utilities, and automotive interior and exterior parts (e.g., composite inserts, trunks, headliners, spare wheel covers, parcel trays, etc.) [48,49,50,51,52,3]. An example is Refine® Hemp-PP for the inserts and top roll of the door panels in the Peugeot 308, and the NAFILean™ used as a bio-composite in the dashboard of the Alfa Roméo Giulia [53]. The hybrid bio-composites could also be used in aerospace components (e.g. non-structural components requiring specific properties), and consumer products (e.g. briefcases, glasses, household items, and appliances).

2. Materials and methods

2.1. Materials

Flax and hemp fibers, with a length of 0.4–1 mm, are used as reinforcement. They were purchased from FRD Company (Troyes, France). Density and mechanical properties were selected to distinguish the two types of fibers. Table 1 summarizes the physical properties of the selected fibers.

Polypropylene (PP) supplied by Repsol Company, under the commercial reference ISPLEN PR580C2M, with a melting temperature of 165 °C, was selected as the matrix for this composite. The melt flow index of this PP injection grade is 20 g/10 min at 230 °C (under a load of 2,16 kg) and the density is 905 Kg/m^3.

Fig. 1 shows the natural short fiber (Flax and Hemp), the thermoplastic polymer (polypropylene), and their developed hybrid composite.

2.2. Compounding and injection molding processes

An implementation to elaborate short fiber thermoplastic (SFT) semi-product with different weight fractions of flax and hemp fibers is conducted by compounding neat polypropylene with the two fibers. Three different concentrations of natural fibers (10, 20 and 30 wt.%) were mechanically blended with polypropylene using a Coperion ZSK 18 MEGAlab co-rotating twin-screw (CRT) (screw diameter = 18 mm, L/d = 40) with a weight flow rate of 10 kg/h and a max screw rate of 1200 rpm for the polymer feed. Fibers were introduced separately into the 4th zone using a side feeder screw. The temperatures of the 10 heating zones of the CRT extruder were 170 °C, 190 °C, 200 °C, 200 °C, 210 °C, 200 °C, 200 °C, 190 °C, 180 °C, 180 °C. The extrudates were then cooled down in a cold-water container and pelletized into pellets of 2–3 mm length. Table 2 collates the composition of the studied compounds.

The SFT compounds were injection molded into plates with a square of side 10 cm using Krauss-Maffei machine, with an injection capacity of 156 cm^3 and closure force of 110 tons. The process temperature was fixed at 190 °C in the barrel and at 210 °C at the nozzle while the mold was maintained at 40 °C. The plates were then cut into dumbbell-shaped specimens for different experimental tests.

2.3. Characterization techniques

2.3.1. Geometric parameters verification

Fiber length measurements before and after extrusion and injection processing were carried out on extracted fibers using a Leica Microsystems optical microscope. The obtained fiber's images were converted into vector graphics using Inkscape® software and then the overall fiber and length distributions were evaluated using a developed Python program. A 12 h Soxhlet extraction was used to dissolve the PP matrix with xylene solvent, and then extract flax and/or hemp fibers.

Table 1
Physical properties of flax and hemp fibers.

	Density (g/cm^3)	Tensile modulus (GPa)	Breaking stress (MPa)	Breaking strain (%)
Flax	1.4	40–85	800–2000	2.1–3
Hemp	1.48	26–44	500–900	7.6–1.8

2.3.2. Mechanical testing

Injection molded plates were cut into dumbbell-shaped specimens according to ISO 527–2 1BA standard using a Speedy 400™ Trotec laser cutter machine. The cut angles are 0°, 45° and 90° with respect to the injection flow direction as shown in Fig. 2. These angles were chosen to evaluate fiber orientation influence on the composite behavior. It is important to note that more cut angles (other than 0, 45, and 90°) may be explored and a parametric study on the effect of cut angles on the mechanical performance of the developed composites may be evaluated. The tensile tests were carried out using a Shimadzu AGX-V testing machine equipped with 50KN load cell. All the tests were performed at room conditions which were 23 °C temperature and 50 % relative humidity. Two strain rates were applied for monotonic tensile tests: low rate $3 \times 10^{-3}\, s^{-1}$ (denoted V3) and high rate $9.7 \times 10^{-2}\, s^{-1}$ (denoted V1). In the case of loading-unloading tensile tests only the low strain rate, V3, was applied for both loading and unloading steps. At least three specimens were tested and only the results that seemed to be more realistic were selected.

2.3.3. Morphological testing

The morphology of cryo-fractured surfaces of 16 samples was examined using a JEOL, JSM 6510 LV scanning electron microscope (SEM) operating at 10–20 kV. The cryo-fractured surfaces were acquired from injection-molded bars and then coated with a coating of gold using an argon plasma metallizer from PELCO 91,000.

3. Results and discussion

3.1. Fiber's length measurements

The combined impact of melt-processing and fiber hybridization on the fiber's length distribution for fiber-hybrid and non-hybrid composite samples was investigated. Fig. 3 shows the fiber's length distribution curves for extracted hybrid and non-hybrid fibers as compared to the virgin flax and hemp fibers. One can observe that the length distribution of virgin hemp fibers is wider, suggesting a heterogeneous composition in terms of fiber length. In contrast, virgin flax fibers have a more concentrated distribution, with a peak at a shorter fiber length of about 0.3 mm, indicating a more uniform composition of fiber sizes in flax fibers. Interestingly, the distribution curves of the fibers extracted from the composites show a noticeable change in fiber lengths post-processing. Indeed, regardless of the fiber's type, it is clearly seen that the melt processing steps significantly affects the length of the fibers, resulting in a more uniform and narrowed fibers distribution, particularly in the fiber-hybrid samples for the same fiber's content (10 wt%), the average length of fibers was found to be 0.48 ± 0.31 mm for the extracted hemp/flax hybrid, whereas it was 0.62 ± 0.33 mm for the non-hybrid flax and hemp fibers. This reduction in the length for hybrid fibers could be explained by a higher interaction and entanglement between flax and hemp fibers, leading to a more fiber-fiber collision and subsequent breakage during the melt processes steps [54]. In addition, the decrease in fiber length may also be due to the temperature and shearing forces used during the twin-screw extrusion process, which indicates that the fibers have lower thermal stability compared to the PP matrix.

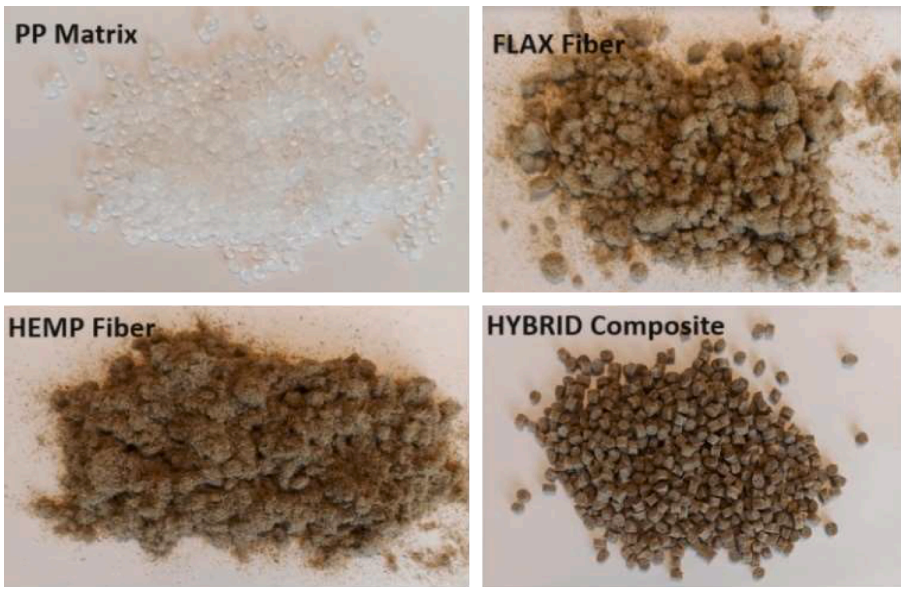

Fig. 1. Polypropylene matrix, Flax and Hemp fibers, and their PP/Flax/Hemp hybrid composite.

Table 2
Composition of the different studied compounds.

Batch	Composition	Weight fraction flax (wt%)	Weight fraction hemp (wt%)
Neat PP	PP	0	0
F10	PP+FLAX	10	0
H10	PP+HEMP	0	10
FH10	PP+FLAX+HEMP	5	5
FH20	PP+FLAX+HEMP	10	10
FH30	PP+FLAX+HEMP	15	15

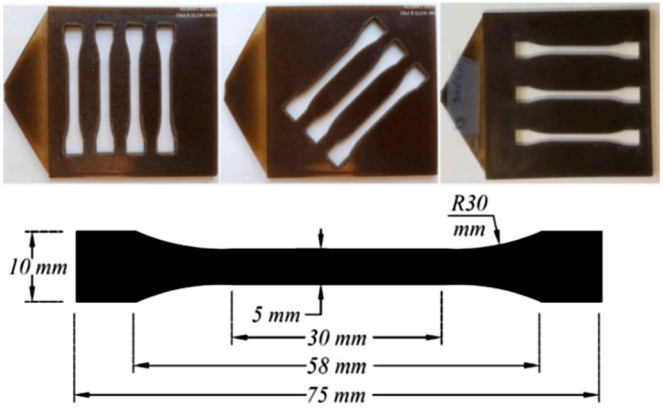

Fig. 2. Plates cut in dumbbell-shaped specimens according to ISO 527–2 Standard at 0°, 45° and 90° with respect to the injection molding flow direction.

3.2. Mechanical properties

3.2.1. Effect of fiber orientation on the fiber-hybrid composite's mechanical behavior

Fig. 4 depicts tensile stress-strain curves of flax/hemp fiber-hybrid composite with two fiber contents: 20 wt% (Fig. 4a) and 30 wt% (Fig. 4b). Specimens were cut at 0°, 45° and 90° with respect to the injection molding flow direction (IFD) and loaded at a strain rate equals to $9.7 \times 10^{-2}\ s^{-1}$. For both fiber contents, one can clearly see the influence of the fiber orientation on the composite behavior by comparing

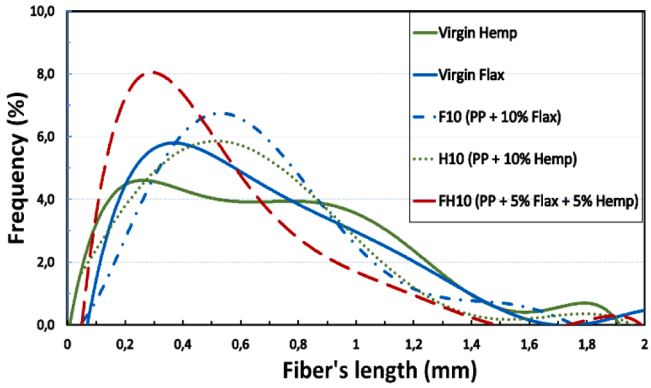

Fig. 3. Distribution of fiber's length before and after injection molding process.

the mechanical responses of the three cut angles. Both the elastic stiffness and the tensile strength are higher for 0° cut angle specimens than those of the specimens cut at 45° and 90° This could be related to the typical non-uniformity of fiber orientation distribution that characterizes the injection molded composite parts. Indeed, the fiber orientation distribution can vary significantly either across the parts' thickness or near their edges. It has been demonstrated that the thickness of injection molded parts made of short glass-fiber reinforced thermoplastics shows a shell/core/shell structure [55,56]. In shell layers, fibers are mainly oriented in the IFD whereas, inside the core layer, fiber orientation becomes orthogonal to the IFD. In the case of short natural fibers composites, particularly with PP matrix, several studies have tried to better understand the microstructure of such composites [57,58,59,60,61]. In these studies, it has been proven that the fibers are arranged in layers like composites with short glass fibers, however determining the thicknesses of these layers remains a delicate task. Furthermore, fiber orientation distribution, inside the layers, depends on various influencing factors such as injection molding conditions, fiber's aspect ratios and fiber content. It has also been shown that usually fibers in the shell layers, which might be subdivided into two sublayers called skin and shear/transition zone [59], are mainly oriented parallel to the IFD while in the core layer, fibers orientation can vary from parallel to the IFD to random. In the case of the samples cut at 45°, one can note that the strength is lower than that of dumbbells cut at 90° This can be explained

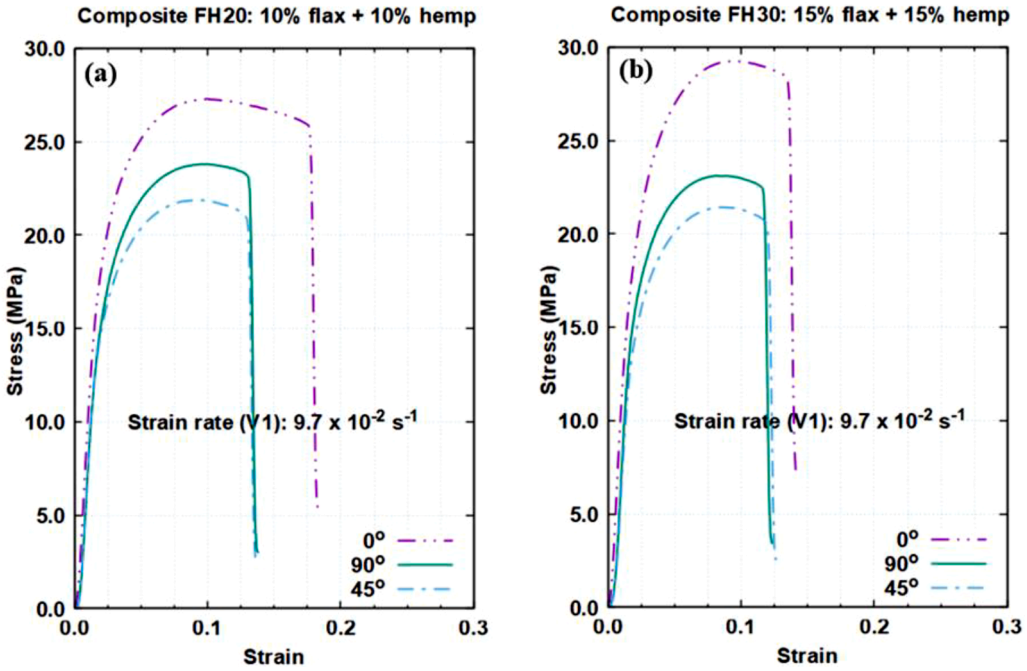

Fig. 4. Effect of fiber orientation on the fiber-hybrid composite's mechanical behavior (strain rate equals $9.7 \times 10^{-2}\, s^{-1}$). (a) Composite FH20 (b) Composite FH30.

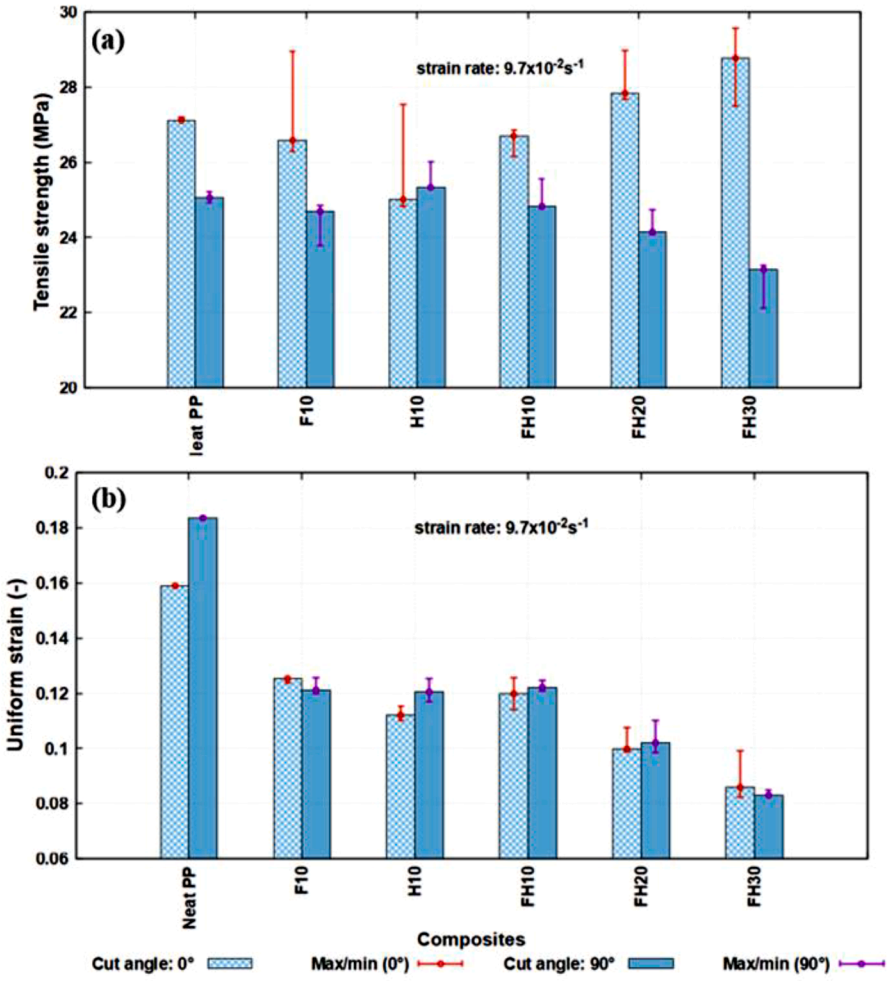

Fig. 5. Tensile strengths and uniform strains obtained from stress-strain curves of neat PP, non-hybrid and fiber-hybrid composites loaded at $9.7 \times 10^{-2}\, s^{-1}$ strain rate for specimens cut at 0° and 90° angle. (a) Tensile strength stress. (b) Uniform strain.

by the fact that, whether in the skins or in the core layer, only a small number of fibers are parallel to the IFD and the remaining fibers are probably oriented at 45°, resulting in a decrease of the mechanical resistance.

Tensile strengths and uniform strains of neat PP and all fiber-hybrid and non-hybrid composites for two cut angles 0° and 90° are shown in Fig. 5. One can clearly note that neat PP and its composites display a higher tensile strength for specimens cut at 0° than those cut at 90° In the case of neat PP, results show an anisotropic behavior. Indeed, several studies [62,63,64,65] have shown that injection molding PP is highly anisotropic and presents a multilayer crystalline structure throughout the thickness. Each layer is characterized by a specific orientation distribution of molecular chains with respect to the IFD. These studies have also revealed that the chain orientation distributions, which are very sensitive to injection molding conditions, have an important influence on the mechanical performance of the final PP parts.

However, in the case of thermoplastic composites, when comparing tensile strength values of non-hybrid composites with 10wt% of flax and hemp fibers (F10 and H10 respectively), it can be seen that the tensile strength of the samples cut at 0° significantly higher for F10 than that for H10. On the other hand, for dumbbells cut at 90° the composite H10 exhibits a higher tensile strength than that of the composite F10 cut at the same angle. This could be explained by the variation of shell/core layers in the composites, i.e. shell layer in the composite F10 is thicker than that of the composite H10, which results in more fibers oriented parallel to the IFD and vis-versa for the core layer.

Young's moduli data of neat PP and all composites are shown in Fig. 6. It is observed that neat PP samples cut at 0° are stiffer than those cut at 90° As explained before, this can be due to the crystalline chain orientation repartition throughout the thickness [62,63,64,65]. On the other hand, Young's moduli for both hybrid and non-hybrid composites with 10% wt fibers are similar, which can be explained by the significant decrease in the average fiber's length observed for the FH10 samples (see Fig. 5). Compared to the F10, H10 and FH10 composites, FH20 and FH30 fiber-hybrid composites exhibit an increase in Young's modulus for either 0° or 90° cut angle dumbbells. This can be explained by the higher fiber mass fraction.

3.2.2. *Effect of the fiber hybridization and content on the mechanical behavior of hybrid composites*

To highlight the effect of combining two different natural fibers on the overall composite mechanical behavior, uniaxial tensile tests on fiber-hybrid and non-hybrid composites with the same fiber weight fraction were carried out. Fig. 7a presents stress-strain curves of non-hybrid F10 and H10 composites (with 10 wt.% of flax fiber and 10 wt. % of hemp fiber, respectively) and fiber-hybrid composite FH10 (with 5 wt.% short flax and 5 wt.% short hemp fibers). Although these samples have the same fiber content, fiber-hybrid composite shows intermediate properties for both the stiffness and the tensile strength compared with non-hybrid composite. Fig. 7b shows stress-strain curves of the fiber-hybrid composites with three fiber weight fractions: FH10 (5 wt% flax + 5 wt% hemp), FH20 (10 wt% flax +10 wt% hemp) and FH30 (15 wt% flax + 15 wt% hemp). It is clearly shown that increasing fiber mass fraction enhances the composite stiffness and strength but decreases the strain at failure.

Fig. 8 illustrates the effect of the strain rate on the fiber-hybrid composite behavior. One can observe the elasto-viscoplastic aspect that characterizes the composite behavior. It is shown that the viscoplasticity is dependent on fiber content as it becomes more pronounced with an increase in fiber content.

3.2.3. *Mechanical damage evolution inside the composites*

Fig. 9 presents loading-unloading tensile curves including an estimate of damage for each loop. Loading-unloading tensile tests were carried out on non-hybrid (F10 and H10) composites and hybrid composite FH10 at the same cut angle (0°) and strain rate (V3). The damage variable is identified by the decrease of stiffness according to the continuum damage mechanics (i.e. $d = 1\text{-}E/E0$ with E0 and E are the initial and the current Young's moduli, respectively). To determine the current Young's modulus E, the slope of a straight line connecting the hysteresis intersection points for each loop was measured. From Fig. 9, one can notice that damage values increase where stresses at unloading strains are more important. For instance, damage in flax composite (F10) shows higher values in comparison with those of hemp composite (H10). The same remark can be made for hybrid-fiber composite FH10. Besides, the level of hybrid composite damage is relatively significant even at a low unload strain of 0.02. This could be related to the weakness of the fiber/matrix interface due to the different origins of the fibers and the matrix as it was demonstrated by SEM images (Fig. 10).

Fig. 10 presents SEM images taken on the surface and the cross-section fracture of the FH10 hybrid composite dumbbell. Fig. 10a shows the case of a dumbbell cut at 0° One can see the print of fibers that are mainly oriented parallel to the IFD which corroborates previous studies [61,66] demonstrating that the main vegetal fibers in the skin

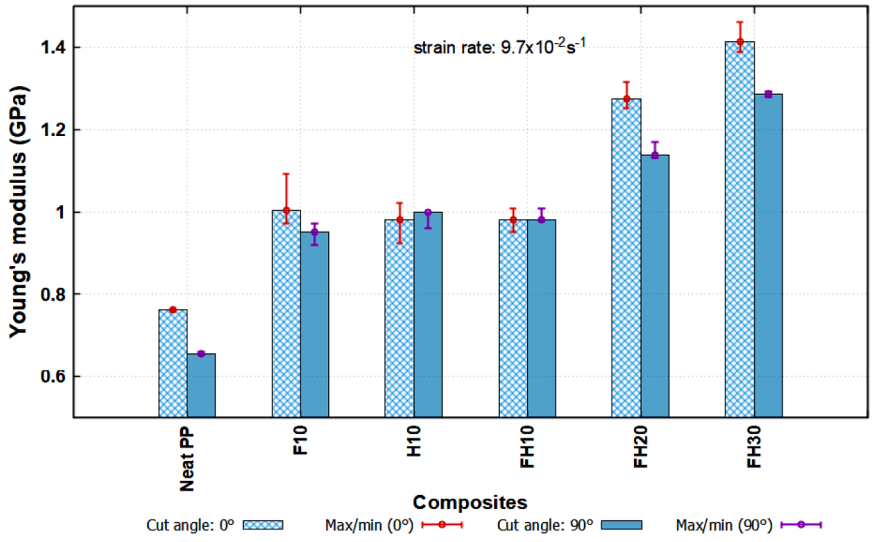

Fig. 6. Young's modulus of neat PP and composites F10, H10, FH10, FH20 and FH30 obtained from strain-stress curves obtained at a strain rate $9.7 \times 10^{-2}\ s^{-1}$ for specimens cut at 0° and 90° angles.

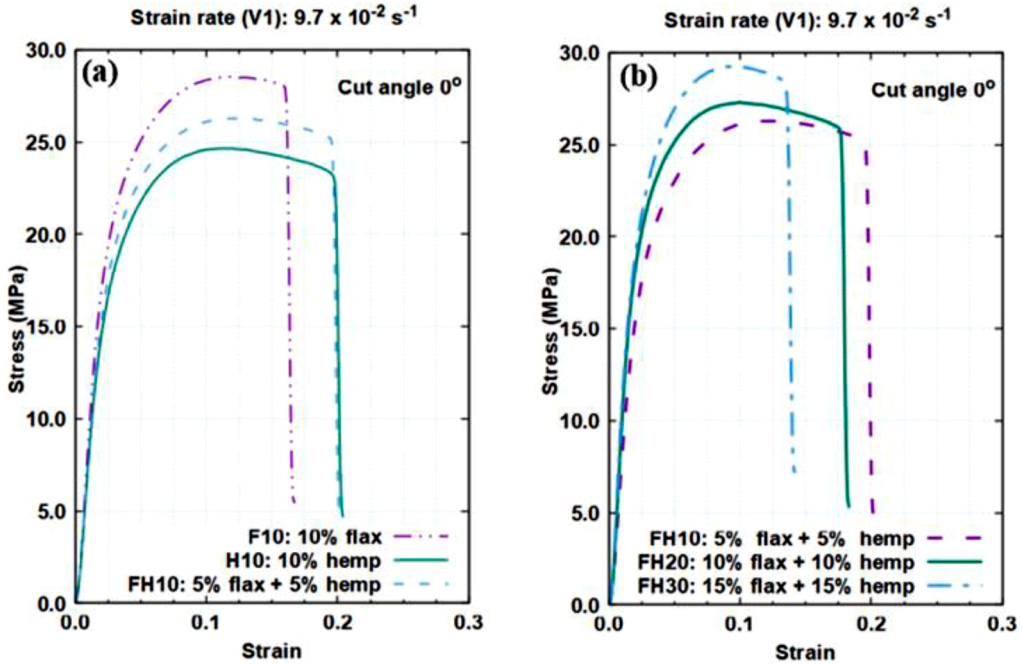

Fig. 7. Uniaxial tensile curves at the strain rate of $9.7 \times 10^{-2}\ s^{-1}$ and 0° cut angle. (a) Effect of the fiber hybridization, and (b) Effect of the fiber-hybrid mass fractions.

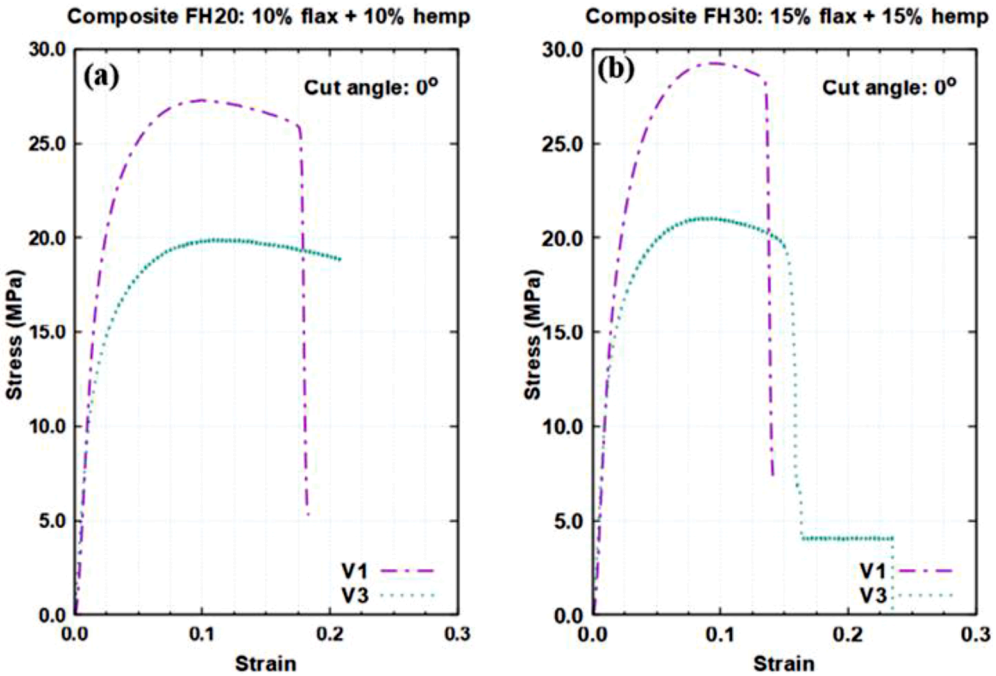

Fig. 8. Tensile curves of composites a) FH20 and b) FH30 at different strain rates: $9.7 \times 10^{-2} s^{-1}$ (V1) and $3 \times 10^{-3}\ s^{-1}$ (V3).

layer have the IFD orientation. One can also observe that there are no visible cracks at the surface, suggesting that damage initiations are likely occurring in the inner layers throughout the dumbbell thickness, particularly in the core layer. On the other hand, Fig. 10b displays the SEM image of a dumbbell cut at 90° An important detail revealed by this figure is the crack at the surface, indicating fiber decohesion inside the dumbbell. This implies that contrary to a dumbbell cut at 0°, damage initiates in the skin layer in the matrix and at the interfaces of fibers which are perpendicularly oriented to the loading direction.

Furthermore, Fig. 10c and 10d show SEM pictures of the fracture surfaces of dumbbells cut at 0° and at 90° relative to the IFD, respectively. It is evident that the main damage aspects are fiber-matrix debonding, matrix microcracking, and fiber pull-out. However, fiber breakage cannot be confirmed primarily for two reasons. Firstly, the weak bonds between the matrix and the fibers result in no scraps of PP remaining attached to the pulled-out fiber's side, mainly due to the absence of fiber treatments aimed at enhancing matrix/fiber bonds. Secondly, the relatively high strength of the fibers compared to the adhesion strength further complicates the confirmation of fiber breakage.

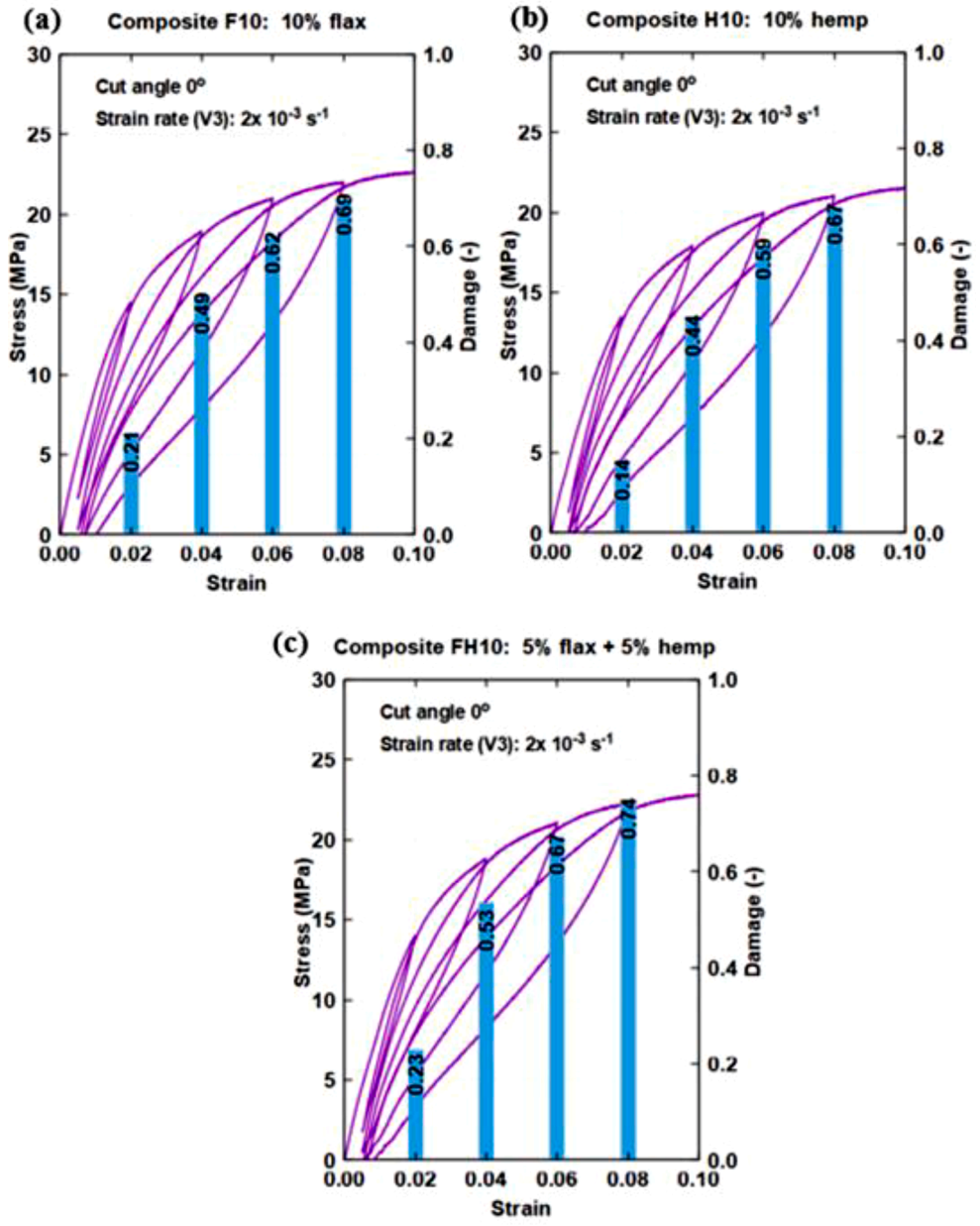

Fig. 9. Loading-unloading tensile curves with damage estimate: (a) Composite F10, (b) Composite H10 and (c) composite FH10. All dumbbells were cut at 0° and tested at the same strain rate: $2 \times 10^{-3}\, s^{-1}$ (V3).

3.3. Macromechanical modeling

The experimental results obtained in section 3.2 have shown that the mechanical behavior of the hybrid composites is sensitive to strain rates, whatever the composition of the mixture and the cutting angle of the samples. In this modeling, it is assumed that viscoplasticity predominates over damage, especially during the work-hardening phase, remaining far from the softening phase. As a result, varying the strain rate has an important impact on both tensile strength and uniform strain, without significantly influencing the material's stiffness.

The modeling of viscoplasticity as a rheological phenomenon can be incorporated into calculations using a range of approaches, each offering different levels of accuracy and precision. In this study, a simple elasto-viscoplastic constitutive law was applied to model the mechanical behavior of the PP/flax/hemp hybrid composite. This decision is motivated by multiple factors. The model, widely employed in the context of metallic materials [67,68,69], has been successfully adapted for polymer materials, particularly thermoplastic polymers. The effectiveness of Perzyna's viscoplastic model in predicting the nonlinear viscous behavior of thermoplastic polymers is well-documented in various studies [70,71]. In the present work, the model was directly applied to the PP/flax/hemp hybrid composite bypassing the need for homogenization methods [72,73], which typically require an understanding of the behaviors of both phases (i.e. matrix and inclusions) along with various parameters such as volume fraction of each phase, aspect ratio, reinforcement orientation, etc. Adopting this direct approach simplifies the modeling process by reducing the number of parameters that need to be identified, thus making it more user-friendly. In the following, the basic assumptions of this model are described in this section, together with a concrete application on the composite for specimens cut at 0° to the injection direction, for different weight fractions of fiber-hybrid (10, 20 and 30 %) and for different strain rates (V1 and V3).

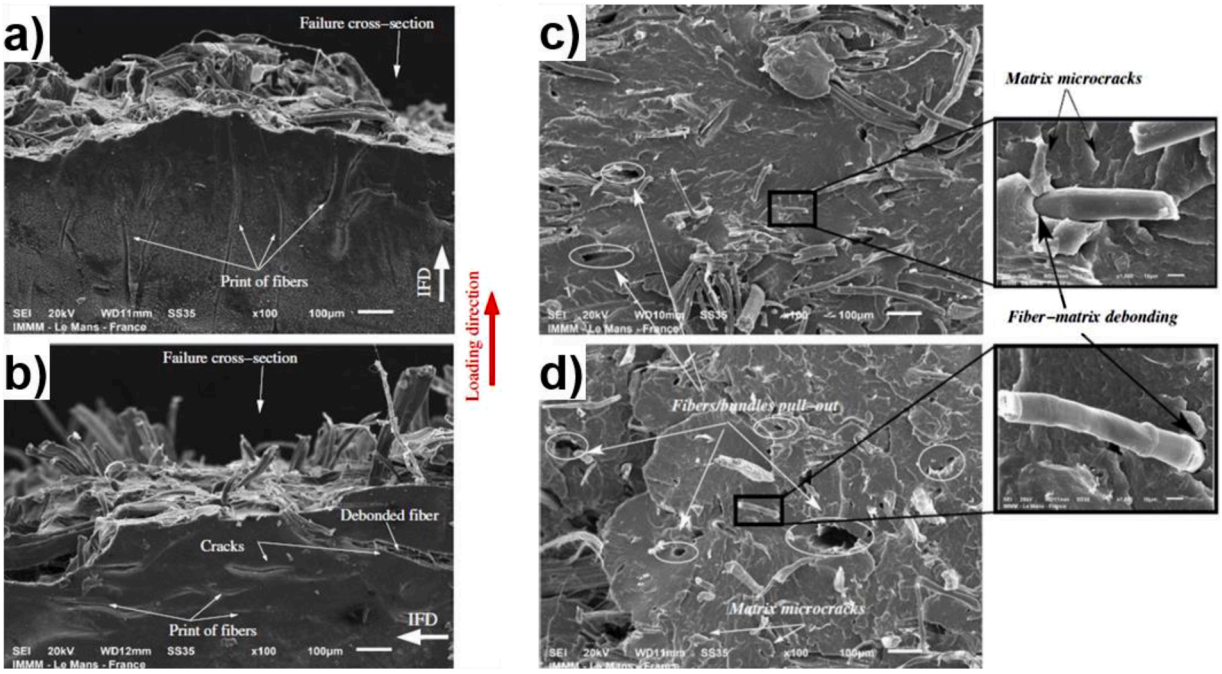

Fig. 10. SEM images showing dumbbell surface and cross-section fracture of hybrid composite FH10: (a and c) Dumbbell cut at 0°, (b and d) dumbbell cut at 90° (at strain rate of $9.7 \times 10^{-2}\, s^{-1}$ - V1).

3.3.1. Total strain decomposition

A three-dimensional elasto-viscoplastic model assumes that the total strain tensor is subdivided into elastic (ε^{el}) and inelastic (ε^{in}) portions:

$$\boldsymbol{\varepsilon} = \boldsymbol{\varepsilon}^{el} + \boldsymbol{\varepsilon}^{in} \tag{1}$$

and the stress-strain rate relation is derived from:

$$\dot{\boldsymbol{\sigma}} = \boldsymbol{C}^{el} : \dot{\boldsymbol{\varepsilon}}^{el} = \boldsymbol{C}^{el} : \left(\dot{\boldsymbol{\varepsilon}} - \dot{\boldsymbol{\varepsilon}}^{in}\right) \tag{2}$$

where C^{el} is the fourth-order elastic stiffness operator.

3.3.2. Perzyna elasto-viscoplastic constitutive model

The Perzyna-type elasto-viscoplastic constitutive model [67,68] is used for the simulations presented in this work. This theory was initially developed for metals, before being extended to modeling the viscoplastic behavior of geomaterials and thermoplastics polymers. It considers an isotropic, pressure-independent, viscoplastic response. In this case, $\boldsymbol{\varepsilon}^{in}$ is denoted $\boldsymbol{\varepsilon}^{vp}$ and the yield criterion is:

$$f\left(\sigma_{eq}, p\right) \equiv \sigma_{eq} - \left(\sigma_y + R(p)\right) \tag{3}$$

where σ_{eq} is the Von Mises equivalent stress, $R(p)$ is the hardening function and σ_y is the initial stress. The yield function is negative for elastic deformation, and it may be positive for viscoplastic deformation.

The three hardening functions defined hereafter require two parameters: the hardening modulus (k [Pa]) and the hardening exponent (n [-]):

$$R(p) = \begin{cases} \begin{cases} \text{linear hardening}: \ R(p) = k\,p \\ \text{powerlawhardening}: R(p) = k\,p^{n} \\ \text{exponential law hardening}: \ R(p) = k[1 - e^{-np}] \end{cases} & \text{if } p \succ 0 \\ 0, \quad \text{otherwise} \end{cases} \tag{4}$$

The accumulated plasticity p is an internal variable of the model which keeps track of the past history undergone by the material and is linked to the viscoplastic law:

$$p(\tau) = \int_0^{\tau} \dot{p}(t)\, dt \quad \text{and} \quad \dot{p} = \left(\frac{2}{3}\dot{\boldsymbol{\varepsilon}}^{vp} : \dot{\boldsymbol{\varepsilon}}^{vp}\right)^{1/2} \tag{5}$$

As in elasto-plasticity, the inelastic strain rate is governed by a flow rule:

$$\dot{\boldsymbol{\varepsilon}}^{vp} = \dot{p}\frac{\partial f}{\partial \boldsymbol{\sigma}} = \dot{p}\,\frac{3}{2}\,\frac{\boldsymbol{s}}{\sigma_{eq}} \quad \text{whichimplies} tr(\dot{\boldsymbol{\varepsilon}}^{vp}) = 0 \tag{6}$$

However, the multiplier $\dot{p}$is not defined by a consistency condition. A viscoplastic function is used instead:

$$\dot{p} = g_v\left(\sigma_{eq}, p\right) \succ 0 \ \ if\ f \succ 0 \quad ; \quad \dot{p} = 0 \ \ if\ f \leq 0 \tag{7}$$

The two viscoplastic functions defined hereafter require two parameters: the viscoplastic modulus (η [Pa.s] or κ [1/s]) and the viscoplastic exponent m[-]:

Ø Norton's viscoplastic power law:

$$g_v\left(\sigma_{eq}, p\right) = \begin{cases} \dfrac{\sigma_y}{\eta}\left(\dfrac{f}{\sigma_y}\right)^{m} & if\ f \succ 0 \\ 0, \quad \text{otherwise} \end{cases} \tag{8}$$

Ø Viscoplastic power law as defined in ABAQUS [69]. This law is obtained by a slight modification of Norton's power law:

$$g_v\left(\sigma_{eq}, p\right) = \begin{cases} \kappa\left(\dfrac{f}{\sigma_y + R(p)}\right)^{m} & \text{iff} \succ 0 \\ 0, \text{otherwise} \end{cases} \tag{9}$$

3.3.3. Analytical based fitting method

An inverse method is used for parameter identification in viscoplastic deformation. This inverse solution procedure consists of an optimization method allowing adjustment of the parameters so that the calculated response matches the one measured in a uniaxial tensile test. For Perzyna constitutive model it is shown that the yield criterion is given in

viscoplastic deformation as follows:

$$f(\sigma_{eq}, p) \equiv \sigma_{eq} - (\sigma_y + R(p)) = \sigma_v \succ 0 \tag{10}$$

Consider a monotonic uniaxial tension test such that σ_{11} is the only non-zero component. The Von Mises equivalent stress is given by:

$$\sigma_{eq} = \sqrt{\frac{3}{2}\boldsymbol{s} : \boldsymbol{s}} = \sigma_{11} \tag{11}$$

Using Eqs. (1.8), (1.9), (1.10) and (1.11), the viscous stress σ_v is written as:

$$\sigma_v = \begin{cases} \sigma_y \left(\dfrac{\eta \dot{p}}{\sigma_y}\right)^{1/m} \text{(Using Norton's VP power law)} \\ (\sigma_y + R(p)) \left(\dfrac{\dot{p}}{\kappa}\right)^{1/m} \text{(Using VP power law as defined in Abaqus)} \end{cases} \tag{12}$$

Finally, using Eqs. (1.11) and (1.12), the uniaxial stress is given as follows:

$$\sigma_{11}^{Fitted} = \sigma_y + R(p) + \sigma_v \tag{13}$$

$$\text{where} : \begin{cases} p = \varepsilon^{vp} = \varepsilon - \dfrac{\sigma^{exp}}{E} \\ \dot{p} = \dfrac{p_{n+1} - p_n}{\Delta t} = \dot{\varepsilon} \dfrac{p_{n+1} - p_n}{\varepsilon_{n+1} - \varepsilon_n} \end{cases} \tag{14}$$

σ^{exp} is the experimentally measured stress and σ_{11}^{Fitted} is the fitted engineering stress. In the previous equation there are five parameters to be determined: yield stress (σ_y), two parameters for the hardening function (k and n), and two parameters for the viscoplastic function (η or κ, and m). The optimization minimizes an objective function which is formed from the square of the difference between measured and simulated stress response for the considered uniaxial tensile test. The sum of squared differences (SSD) between the analytical results and the measured data can be calculated as:

$$SSD = \sum_{i=1}^{N} \left(\sigma_i^{exp} - \sigma_{11_i}^{Fitted}\right)^2 \tag{15}$$

where σ_i^{exp} are the measured stress value data, $\sigma_{11_i}^{Fitted}$ are the stress values obtained from analytical simulation, while N stands for the number of data points.

3.3.4. Fitting results

To study the performance of the Perzyna elasto-viscoplastic constitutive model, six different combinations are considered, each time choosing a hardening stress function and a viscoplastic function as follows:

(1): LHNVP (Linear hardening + Norton's VP power law)
(2): PHNVP (power law hardening + Norton's VP power law)
(3): EHNVP (Exponential law hardening + Norton's VP power law)
(4): LHAVP (Linear hardening + Abaqus VP power law)
(5): PHAVP (power law hardening + Abaqus VP power law)
(6): EHAVP (Exponential law hardening + Abaqus VP power law)

The fitted material parameters of the six combinations are listed in Table 3. E refers to the Young's modulus, ν is the Poisson's ratio (since the uniaxial stress response is independent of the Poisson ratio, the latter is left undetermined), σ_y is the yield stress, k is the hardening modulus, n is the hardening exponent, η and κ are the viscoplastic modulus and m is the viscoplastic exponent.

Fig. 11 compares experiment results and the response predicted by Perzyna elasto-viscoplastic model for uniaxial tension test for specimens cut at 0° at strain rates of $9.7 \times 10^{-2}\, s^{-1}$ (V1) and $2 \times 10^{-3}\, s^{-1}$ (V3). Material behavior is rate-dependent and is highly nonlinear. The Cauchy stress tensor is used as stress measure and the nominal strain as strain measure.

The results show, that the Perzyna constitutive model can characterize the elasto-viscoplastic behavior of the investigated FH10 hybrid composite with adequate accuracy using the exponential hardening law combined with Norton's viscoplastic power law as shown in Fig. 12.

To better understand the obtained results, the impact of the parameter n of the hardening function on the stress-strain relationship of the composite was evaluated. Three values of hardening exponent n are considered: (i) $n = 1$ which corresponds to a linear hardening, (ii) $n = 0.35$ and $n = 60$ which corresponds to a nonlinear hardening. The evolution of the hardening functions (linear, power, and exponential laws) for different values of n are plotted in Fig. 13. It can be shown that the exponential law hardening with high values of n reproduces the real behavior of the hybrid composites, i.e., nonlinear behavior followed by a constant stress in the viscoplastic domain. This explains better the analytical results obtained with the exponential law hardening as shown in Fig. 11.

To apply Perzyna's elasto-viscoplastic constitutive approach to model the macroscopic behavior of FH20 and FH30 hybrid composites, a parametric study was carried out to investigate the evolution of Young's modulus (E) and yield stress (σ_y) as a function of fiber-hybrid mass fraction (see Fig. 14). In this figure, experimental measurements are represented by large dots. Trend curves are shown as dotted lines.

Fig. 15 presents stress-strain curves of fiber-hybrid composites FH10, FH20 and FH30 obtained at the strain rates of $9.7 \times 10^{-2}\, s^{-1}$ (V1) and $3 \times 10^{-3}\, s^{-1}$ (V3). The same material parameters of the exponential law hardening (k and n) and the Norton's VP power law (η and m) are used for the three mixtures. In the following, a concise overview of the distinct material parameters used in the elastic and viscoplastic phases is presented.

Table 3
EVP parameters of FH10 at 23° identified from experimental data (uniaxial tension tests) for specimens cut at 0° Identification method is explained in subSection 4.3.

		LHNVP	PHNVP	EHNVP	LHAVP	PHAVP	EHAVP
E (MPa)		970	970	970	970	970	970
ν		–	–	–	–	–	–
σ_y [MPa]		7.5	7.5	7.5	7.5	7.5	7.5
Linear hardening	k [MPa]	112.81			69.42		
	n [-]	1			1		
Power law hardening	k [MPa]		35.80			33.38	
	n [-]		0.36			0.35	
Exponential law hardening	k [MPa]			11.87			9.51
	n [-]			54.73			56.22
Norton's VP power law	η [MPa.s]	1260	43.47	55.60			
	m [-]	5.72	11.61	2.99			
Abaqus VP power law	κ [1/s]				10	1.15	1.39
	m [-]				36.68	2.10	4.56

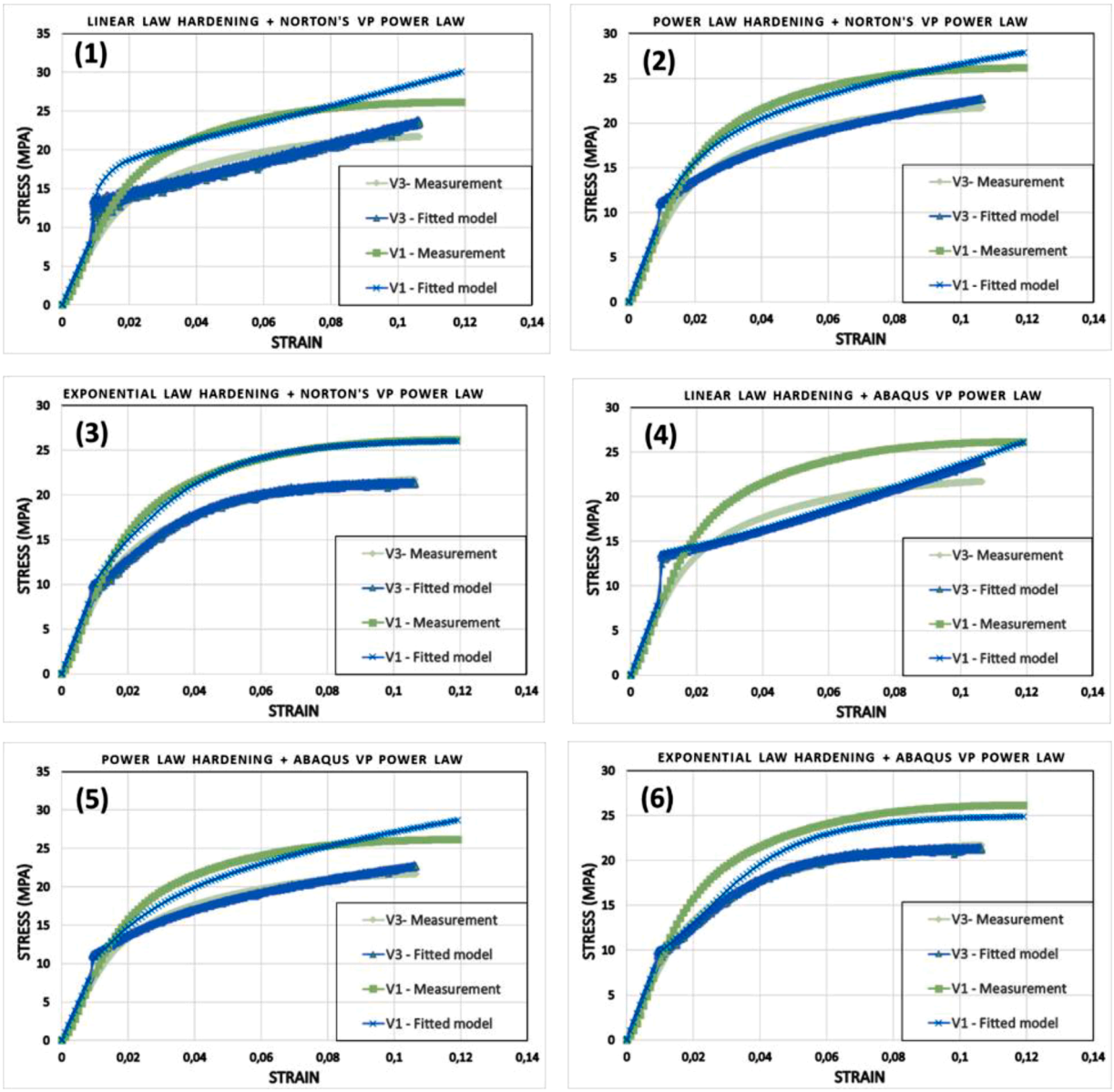

Fig. 11. Comparison of the uniaxial measurement data and the fitted Perzyna elasto-viscoplastic model of FH10 hybrid composite for specimens cut at 0°, and at different strain rates: $9.7 \times 10^{-2}\ s^{-1}$ (V1) and $2 \times 10^{-3}\ s^{-1}$ (V3): (1) LHNVP, (2) PHNVP, (3) EHNVP, (4) LHAVP, (5) PHAVP, (6) EHAVP.

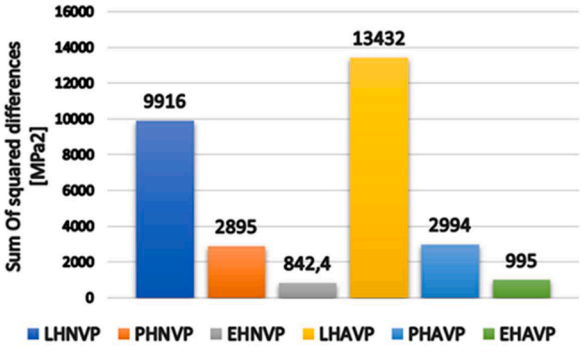

Fig. 12. The sum squared differences (SSD) obtained for the different combinations.

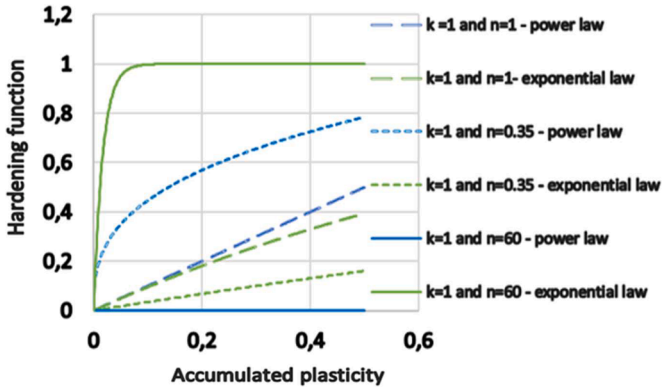

Fig. 13. Impact of the parameter n of the hardening function on the stress-strain relationship.

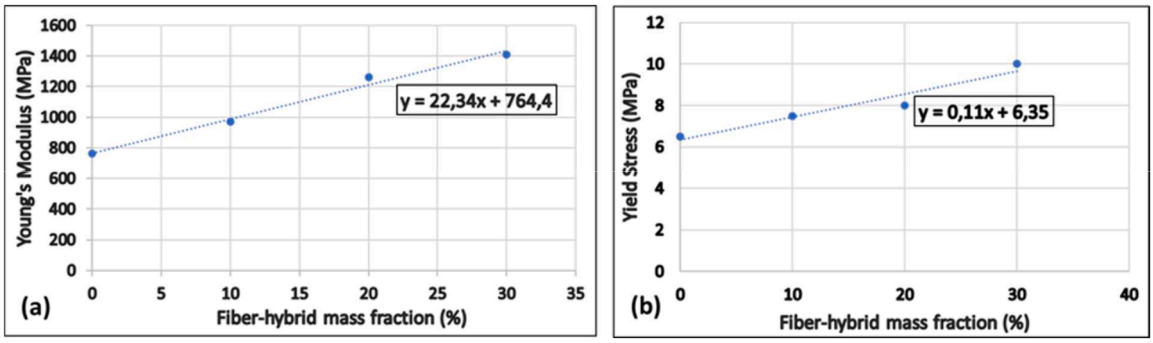

Fig. 14. Experimental (a) Young's Modulus (MPa) and (b) Yield Stress (MPa) as a function of fiber-hybrid mass fraction. Trend curves are drawn as a dashed line.

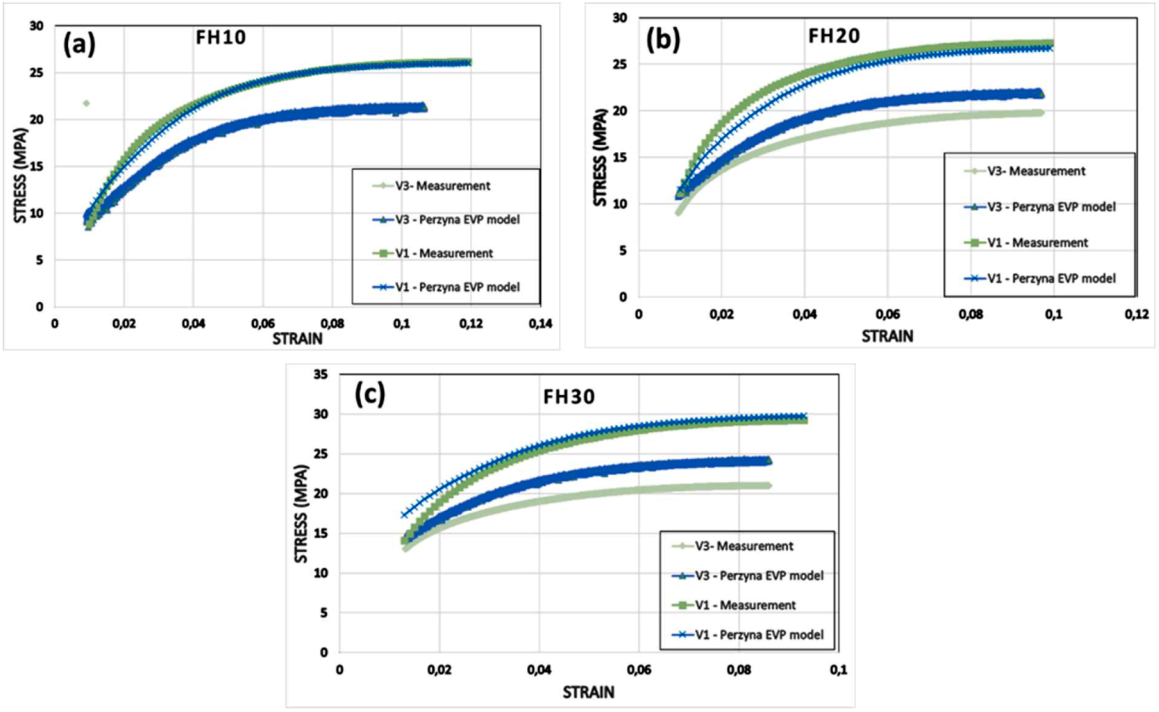

Fig. 15. Tensile curves of composites a) FH10, b) FH20 and c) FH30 at different strain rates: $9.7 \times 10^{-2}\, s^{-1}$ (V1) and $3 \times 10^{-3}\, s^{-1}$ (V3).

$$\begin{cases} x\text{: fiber} - \text{hybridmassfraction}(\%) \\ \text{Young's modulus for the composite } FHx(\text{MPa}) : E_x = 22,34x + 764,4 \\ \text{Yiled stress for the composite } FHx(\text{MPa}) : \sigma_{y_x} = 0,11x + 6,35 \\ \text{Exponential law hardening : } \mathrm{k} = 11,87\text{MPa and n} = 54,73 \\ \text{Norton's VP power law : } \eta = 55,60\text{MPa.s and m} = 2,99 \end{cases}$$

Comparison of the model predictions to experimental uniaxial tensile tests illustrates the necessity to account for the strain rate dependency in the VP deformation regime. The loading curves are clearly nonlinear. This agreement between model and experiment is better with the strain rate of $9.7 \times 10^{-2}\, s^{-1}$ (V1). Less accuracy is observed for low strain rate, even though the curve shape is respected.

It can be found that the perzyna EVP constitutive model is able to capture the mechanical behavior of the tension deformation of hybrid natural short-fiber thermoplastic composites, including the elastic stage, the yield stress, and the nonlinear hardening. In addition, the model has proved its ability to describe the rate dependent behavior of the hybrid composite under tension loading within a wide range of strain rates.

While the simplicity and efficiency of the Perzyna model yield highly satisfactory results, it is essential to acknowledge its inherent limitations. The model's exclusive consideration of isotropic hardening, without accounting for kinematic hardening, presents a notable constraint. Additionally, experimental data frequently displays softening beyond a certain ultimate stress, indicative of a damage-driven behavior. To accurately predict softening behavior, an integration of the Perzyna model with a damage model, such as Chaboche's model [74], becomes imperative. This synergistic approach not only addresses the softening phenomena but also elevates the overall predictive capability of the model, ensuring a more comprehensive representation of material response that the standalone Perzyna model may not fully capture.

4. Conclusion

This research investigated the mechanical performance of thermoplastic composites reinforced with natural hybrid flax/hemp fibers, processed using extrusion techniques, through pure tensile and load/unload tensile tests. The study revealed that the fiber length distribution was significantly impacted by melt processing and injection molding. Specifically, processed hybrid fibers exhibited an average length of 0.48 ± 0.31 mm, whereas non-hybrid fibers measured 0.62 ± 0.33 mm. Furthermore, the orientation of fibers was found to be a critical factor in determining mechanical properties; in the FH30 composite, a change in

fiber orientation from 90° to 0° led to an increase in tensile strength and Young's Modulus by 24.13 % and 10.93 %, respectively. This orientation-dependency was further demonstrated by a 7.89 % increase in tensile strength for 0° specimens between FH10 and FH30 composites. However, a reduction of 30 % in uniform strain was observed. On the other hand, the damage level in hybrid composites (FH10) was found to be more significant than in non-hybrid ones (F10 and H10), due to weaker matrix-fiber bonding in hybrids. This phenomenon was elucidated through SEM observations, showing the progression of cracks and micro-voids in the matrix surrounding the tips of the fibers. Additionally, distinct patterns of micro-crack propagation, debonding, and cohesive failure were observed. These damage mechanisms of the biocomposite are mainly dominated by matrix / fiber debonding, which is likely accompanied by the formation of micro-cracks within the matrix and the pull-out of fibers. Finally, the application of the Perzyna elasto-viscoplastic constitutive model, in conjunction with an analytical parameter fitting strategy, has effectively predicted the behavior of the hybrid composite. This modeling approach, especially when integrated with an exponential hardening law and Norton's viscoplastic power law, yielded the most favorable outcomes and provided a robust tool for understanding and predicting composite behavior.

This study provides a fundamental comprehension of hybrid thermoplastic composites reinforced with natural fibers and proposes that subsequent investigations should concentrate on enhancing the strength of matrix-fiber bonding in order to improve mechanical properties. Recommended approaches include fiber surface treatments and the use of coupling agents like maleated polypropylene (MAPP), which are expected to enhance the fiber/matrix bonding and consequently, improve the composites mechanical properties.

CRediT authorship contribution statement

Bilel Miled: Writing – review & editing, Writing – original draft, Visualization, Validation, Supervision, Methodology, Investigation, Formal analysis, Data curation, Conceptualization. **Slim Kammoun:** Writing – review & editing, Writing – original draft, Visualization, Validation, Methodology, Investigation, Formal analysis, Data curation, Conceptualization. **Imane Belyamani:** Writing – review & editing, Validation, Supervision, Methodology, Investigation, Data curation, Conceptualization. **Laurent Cauret:** Validation, Project administration, Methodology, Conceptualization.

Declaration of competing interest

The authors declare that they have no known competing financial interests or personal relationships that could have appeared to influence the work reported in this paper.

Data availability

Data will be made available on request.

Acknowledgments

The authors express their gratitude to the apprentices of Polyvia Formation for their valuable contributions to the execution of various experimental tests conducted in this study: Jeanne Blanchais, Pierre-Louis Ferrara, Sacha Gontier, Jeremy Grondin, Thomas Lefrancois, Rui Feng, Clément Hamon, Luc De Kersabiec, Morgan Menard, and Maxime Palesi.

References

[1] M.R. Sanjay, P. Madhu, M. Jawaid, P. Senthamaraikannan, S. Senthil, S. Pradeep, Characterization and properties of natural fber polymer composites: a comprehensive review, J. Clean. Prod. 172 (2018) 566–581.
[2] O. Faruk, A.K. Bledzki, H.P. Fink, M. Sain, Biocomposites reinforced with natural fbers: 2000-2010, Prog. Polym. Sci. 37 (2012) 1552–1596.
[3] K.L. Pickering, M.G.A. Efendy, T.M. Le, A Review of Recent Developments in Natural Fibre Composites and Their Mechanical Performance, Compos. Part A Appl. Sci. Manuf 83 (2016) 98–112.
[4] S.N.A. Safri, M.T.H. Sultan, M. Jawaid, K. Jayakrishna, Impact behavior of hybrid composites for structural applications: A review, Compos. B Eng. 133 (2018) 112–121.
[5] Y. Zhang, Y. Li, H. Ma, Y.T. al, Tensile and interfacial properties of unidirectional flax/glass fiber reinforced hybrid composites, Compos. Sci. Technol. 88 (2013) 172–177.
[6] E. elver, N. Ucar, T. Gulmez, Effect of stacking sequence on tensile, flexural and thermomechanical properties of hybrid flax/glass and jute/glass thermoset composites, J. Industrial. Text. 48 (2018) 494–520.
[7] V. Fiore, L. Calabrese, T. Scalici, P. Bruzzaniti, A. Valenza, Bearing strength and failure behavior of pinned hybrid glass-flax composite laminates, Polym. Test. 69 (2018) 310–319.
[8] M. Cihan, A.J. Sobey, J.I.R. Blake, Mechanical and dynamic performance of woven flax/E-glass hybrid composites, Compos. Sci. Technol. 172 (2019) 36–42.
[9] C.N. Kumar, M.N. Prabhakar, J.I. Song, Effect of interface in hybrid reinforcement of flax/glass on mechanical properties of vinyl ester composites, Polym. Test. 73 (2019) 404–411.
[10] A.K. Barouni, H.N. Dhakal, Damage investigation and assessment due to low-velocity impact on flax/glass hybrid composite plates, Compos. Struct. 226 (2019) 111224.
[11] H.N. Dhakal, Z.Y. Zhang, R. Guthrie, J. Macmullen, N. Bennett, Development of flax/carbon fibre hybrid composites for enhanced properties, Carbohydr. Polym. 96 (2013) 1–8.
[12] M. Assarar, W. Zouari, H. Sabhi, R. Ayad, J.M. Berthelot, Evaluation of the damping of hybrid carbon-flax reinforced composites, Compos. Struct. 132 (2015) 148–154.
[13] J. Flynn, A. Amiri, C. Ulven, Hybridized carbon and flax fiber composites for tailored performance, Mater. Design 102 (2016) 21–29.
[14] V. Fiore, T. Scalici, L. Calabrese, A. Valenza, E. Proverbio, Effect of external basalt layers on durability behaviour of flax reinforced composites, Compos. B Eng. 84 (2016) 258–265.
[15] I. Zivkovic, C. Fragassa, A. A.Pavlovic, T. Brugo, Influence of moisture absorption on the impact properties of flax, basalt and hybrid flax/basalt fiber reinforced green composites, Compos. B Eng. 111 (2017) 148–164.
[16] C. Fragassa, A. Pavlovic, C. Santulli, Mechanical and impact characterisation of flax and basalt fibre vinylester composites and their hybrids, Compos. B Eng. 137 (2018) 247–259.
[17] F.A. Almansour, H.N. Dhakal, Z.Y. Zhang, Investigation into mode II interlaminar fracture toughness characteristics of flax/basalt reinforced vinyl ester hybrid composites, Compos. Sci. Technol. 154 (2018) 117–127.
[18] B.V. Ramnath, S.J. Kokan, R.N. Raja, R. Sathyanarayanan, C. Elanchzhian, A. R. Prasad, V.M. Manickavagam, Evaluation of mechanical properties of abaca–jute–glass fibre reinforced epoxy composite, Mater. Design 51 (2013) 357–366.
[19] V.S. Srinivasan, S.R. Boopathy, D. Sangeetha, B.V. Rammath, Evaluation of mechanical and thermal properties of banana–flax based natural fibre composite, Mater. Design 60 (2014) 620–627.
[20] B.V. Ramnath, R. Sharavanan, M. Chandrasekaran, C. Elanchezhian, R. Sathyanarayanan, R. Niranjan, S.J. Kokan, Experimental determination of mechanical properties of banana jute hybrid composite, Fibers Polym. 16 (2015) 164–172.
[21] M.A. El-baky, M.A. Attia, M.M. Abdelhaleem, M.A. Hassan, Mechanical characterization of hybrid composites based on flax, basalt and glass fibers, J. Compos. Mater. 54 (2020) 4185–4205.
[22] M.A. El-baky, M.A. Attia, M.M. Abdelhaleem, M.A. Hassan, Flax/basalt/E-glass fibers reinforced epoxy composites with enhanced mechanical properties, J. Nat. Fib. 19 (2022) 954–968.
[23] M.A. Attia, M.A. El-baky, M.M. Abdelhaleem, M.A. Hassan, Hybrid composite laminates reinforced with flax-basalt-glass woven fabrics for lightweight load bearing structures, J. Ind. Text. 51 (2022) 4622–4664.
[24] R. Petrucci, C. Santulli, D. Puglia, F. Sarasini, L. Torre, J.M. Kenny, Mechanical characterisation of hybrid composite laminates based on basalt fibres in combination with flax, hemp and glass fibres manufactured by vacuum infusion, Mater. Design 49 (2013) 728–735.
[25] R. Petrucci, C. Santulli, D. Puglia, E. Nisini, J. Tirillo, L. Torre, G. Minak, J. M. Kenny, Impact and post-impact damage characterization of hybrid composite laminates based on basalt fibres in combination with flax, hemp and glass fibres manufactured by vacuum infusion, Compos. B Eng. 69 (2015) 507–515.
[26] M.A. El-baky, A.E. Alshorbagy, A.M. Alsaeedy, M. Megahed, Fabrication of cost effective fiber metal laminates based on jute and glass fabrics for enhanced mechanical properties, J. Nat. Fib. 19 (2022) 303–318.
[27] M.M. Awd Allah, M.A.A. El-baky, H. Alshahrani, T.A. Sebaey, D.A. Hegazy, Multi attribute decision making through COPRAS on tensile properties of hybrid fiber metal laminate sandwich structures for aerospace and automotive industries, J. Compos. Mater. 57 (2023) 3757–3773.

[28] M.M.A. Allah, D.A. Hegazy, H. Alshahrani, T.A. Sebaey, M.A.A. El-baky, Fiber metal laminates based on natural/synthesis fiber composite for vehicles industry: an experimental comparative study, Fibers and Polymers 24 (2023) 2877–2889.

[29] A. Godara, D. Raabe, Influence of fiber orientation on global mechanical behavior and mesoscale strain localization in a short glass-fiber-reinforced epoxy polymer composite during tensile deformation investigated using digital image correlation, Compos. Sci. Technol. 67 (2007) 2417–2427.

[30] P.J. Herrera-Franco, A. Valadez-González, Mechanical properties of continuous natural fibre-reinforced polymer composites, Compos. Part A Appl. Sci. Manuf. 35 (2004) 339–345.

[31] P.V. Joseph, K. Joseph, S. Thomas, Effect of processing variables on the mechanical properties of sisal-fiber-reinforced polypropylene composites, Compos. Sci. Technol. 59 (1999) 1625–1640.

[32] A. Kelly, W.R. Tyson, Tensile properties of fibre-reinforced metals: copper/tungsten and copper/molybdenum, J. Mech. Phys. Solids. 13 (1965) 329–350.

[33] C.L. Tucker, E. Liang, Stiffness predictions for unidirectional short-fiber composites: review and evaluation, Compos. Sci. Technol. 59 (1999) 655–671.

[34] M. May, M. Nossek, N. Petrinic, S. Hiermaier, K. Thoma, Adaptive multi-scale modeling of high velocity impact on composite panels, Compos. Part A Appl. Sci. Manuf. 58 (2014) 56–64.

[35] H. Sandberg, O. Rydholm, Evaluation of Material Models to Predict Material Failure in LS-DYNA, Master's Diss Solid Mech, 2016.

[36] G. D.S.Chethan, R.S. Gunti, C.S.V. Kumar, Experimental and Numerical Modeling of Hemp-Polyester Composites, Wood is Good (2017) 333–342. Vols.

[37] L. Puecha, K.R. Ramakrishnana, N.L. Moignea, S. Corna, P.R. Slangenb, A.L. Ducc, H. Boudhanid, A. Bergereta, Investigating the impact behaviour of short hemp fibres reinforced polypropylene biocomposites through high speed imaging and finite element modelling, Composites Part A 109 (2018) 428–439.

[38] H. Kebir, R. Ayad, A specific finite element procedure for the analysis of elastic behaviour of short fibre reinforced composites, The Projected Fibre approach, Compos. Struct. 118 (2014) 580–588.

[39] W. Shu, I. Stanciulescu, Computational modeling and multiscale homogenization of short fiber composites considering complex microstructure and imperfect interfaces, Compos. Struct. 306 (2023) 116592.

[40] W.T. Kern, W. Kim, A. Argento, E.C. Lee, D.F. Mielewsk, Finite element analysis and microscopy of natural fiber composites containing microcellular voids, Materials and Design 106 (2016) 285–294.

[41] Y. Pan, Z. Zhong, Modeling of the mechanical degradation induced by moisture absorption in short natural fiber reinforced composites, Compos. Sci. Technol. 103 (2014) 22–27.

[42] J. Modniks, J. Andersons, Modeling the non-linear deformation of a short-flax-fiber-reinforced polymer composite by orientation averaging, Composites: Part B 54 (2013) 188–193.

[43] J. Sliseris, L. Yan, B. Kasal, Numerical modelling of flax short fibre reinforced and flax fibre fabric reinforced polymer composites, Compos. Part B Eng. 89 (2016) 143–154.

[44] L. Boccarusso, D. Fazio, M. Durante, Production of PP Composites Reinforced with Flax and Hemp Woven Mesh Fabrics via Compression Molding, Inventions 7 (2022).

[45] A. Bledzki, H. Fink, Unidirectional hemp and flax EP- and PP-composites: Influence of defined fiber treatments, J. Appl. Polym. Sci. 93 (2004) 2150–2156.

[46] U.K. Vaidya, K.K. Chawla, Processing of fibre reinforced thermoplastic composites, Int. Mater. Rev 53 (2008) 185–218.

[47] T. Haghighatnia, A. Abbasian, J. Morshedian, Hemp fiber reinforced thermoplastic polyurethane composite: an investigation in mechanical properties, Ind. Crop. Prod 108 (2017) 853–863.

[48] H.N. Dhakal, Z. Zhang, The use of hemp fibres as reinforcements in composites, Biofiber. Reinf. Compos. Mater (2015) 86–103.

[49] P. Ranalli, G. Venturi, Hemp as a Raw Material for Industrial Applications, Euphytica 149 (2004) 1–6.

[50] E.M.J. Salentijn, Q. Zhang, S. Amaducci, M. Yang, L.M. Trindade, New Developments in Fiber Hemp (Cannabis Sativa, L.), Breeding. Ind. Crops Prod 68 (2015) 32–41.

[51] P. Gohil, K. Patel, V. Chaudhary, Natural Fiber-Reinforced Polymer Composites: A Comprehensive Study on Machining Characteristics of Hemp Fiber-Reinforced Composites, V," in Biomass, Biopolymer-Based Materials, and Bioenergy (2019) 25–50.

[52] E. Sarikaya, H. Çallioglu, H. Demirel, Production of Epoxy Composites Reinforced by Different Natural Fibers and Their Mechanical Properties, Compos. Part B Eng 167 (2019) 461–466.

[53] G. Crini, E. Lichtfouse, G. Chanet, N.M. Crini, Applications of hemp in textiles, paper industry, insulation and building materials, horticulture, animal nutrition, food and beverages, nutraceuticals, cosmetics and hygiene, medicine, agrochemistry, energy production and environment: a review, Environ. Chem. Lett. 18 (2020) 1451–1476.

[54] N.L. Moigne, V.D. Martien, B. Tatiana, A statistical analysis of fibre size and shape distribution after compounding in composites reinforced by natural fibres, Composites Part A: Applied Science and Manufacturing 42 (2011) 1542–1550.

[55] M.R. Kantz, H.D. Newman, F.H. Stigale, The skin-core morphology and structure–property relationships in injection-molded polypropylene, J. Appl. Polym. Sci. 16 (1972) 1249–1260.

[56] S. Kammoun, I. Doghri, L. Brassart, L. Delannay, Micromechanical modeling of the progressive failure in short glass–fiber reinforced thermoplastics – First Pseudo-Grain Damage model, Composites Part A: Applied Science and Manufacturing 73 (2015) 166–175.

[57] A. Abdennadher, Injection Moulding of Natural Fibre Reinforced Polypropylene: Process, Microstructure and Properties", Paris, France, 2015.

[58] K. Albrecht, E. Baur, H.J. Endres, R. Gente, N. Graupner, M. Koch, M. Neudecker, T. Osswald, P. Schmidtke, S. Wartzack, K. Webelhaus, J. Müssig, Measuring fibre orientation in sisal fibre-reinforced, injection moulded polypropylene – Pros and cons of the experimental methods to validate injection moulding simulation, Composites Part A: Applied Science and Manufacturing 95 (2017) 54–64.

[59] E. Lafranche, V.M. Oliveira, C.I. Martins, P. Krawczak, Prediction of injection-moulded flax fibre reinforced polypropylene tensile properties through a micro-morphology analysis, J. Compos. Mater. 49 (2013) 113–128.

[60] R. Karthikeyan, Analysis of Natural Fiber Orientation in polymer composites Produced by Injection Molding Process", 2017.

[61] T. Aurich, G. Mennig, Flow-induced fiber orientation in injection molded flax fiber reinforced polypropylene, Polym. Compos. 22 (2001) 680–689.

[62] Z. Mencik, D.R. Fitchmun, Texture of injection-molded polypropylene, J. Polym. Sci. 11 (1973) 973–989.

[63] M. Fujiyama, T. Wakino, K. Kawasaki, Structure of skin layer in injection-molded polypropylene, J. Appl. Polym. Sci. 35 (1988) 29–49.

[64] M. Fujiyama, I. Masada, K. Mitani, Melting and crystallization behaviors of injection-molded polypropylene, J. Appl. Polym. Sci. 78 (2000) 1751–1762.

[65] S. Liparoti, V. Speranza, A. Sorrentino, G. Titomanlio, Mechanical Properties Distribution within Polypropylene Injection Molded Samples: Effect of Mold Temperature under Uneven Thermal Conditions, Polymers (Basel) 9 (2017) 585.

[66] A. Bourmaud, G. Ausias, G. Lebrun, M.L. Tachon, C. Baley, Observation of the structure of a composite polypropylene/flax and damage mechanisms under stress, Ind. Crops. Prod. 43 (2013) 225–236.

[67] H. Hallberg, K. Ryttberg, M. Ristinmaa, Model Describing Material-Dependent Deformation Behavior in High-Velocity Metal Forming Processes, J. Eng. Mech. 135 (April 2009) 345–357.

[68] T. Frąś, Z. Nowak, P. Perzyna, R.B. Pęcherski, Identification of the model describing viscoplastic behaviour of high strength metals, Inverse Probl. Sci. Eng. 19 (January 2011) 17–30.

[69] K. Kowalczyk-Gajewska, E.A. Pieczyska, K. Golasiński, M. Maj, S. Kuramoto, T. Furuta, A finite strain elastic-viscoplastic model of Gum Metal, Int. J. Plast. 119 (August 2019) 85–101.

[70] A. Arriaga, R. Pagaldai, A.M. Zaldua, A. Chrysostomou, M. O'Brien, Impact testing and simulation of a polypropylene component. Correlation with strain rate sensitive constitutive models in ANSYS and LS-DYNA, Polym. Test. 29 (April 2010) 170–180.

[71] B. Miled, I. Doghri, L. Delannay, Coupled viscoelastic–viscoplastic modeling of homogeneous and isotropic polymers: Numerical algorithm and analytical solutions, Comput. Methods Appl. Mech. Eng. 200 (November 2011) 3381–3394.

[72] O. PIERARD, I. DOGHRI, An enhanced affine formulation and the corresponding numerical algorithms for the mean-field homogenization of elasto-viscoplastic composites, Int. J. Plast. 22 (January 2006) 131–157.

[73] L. Zhang, W. Yu, A Variational Asymptotic Method for Unit Cell Homogenization of Elasto-Viscoplastic Heterogeneous Materials, in: 54th AIAA/ASME/ASCE/AHS/ASC Structures, Structural Dynamics, and Materials Conference, 2013.

[74] J.F. Maire, J.L. Chaboche, A new formulation of continuum damage mechanics (CDM) for composite materials, Aerosp. Sci. Technol. 1 (June 1997) 247–257.